EFDA–JET–PR(12)61

G. Verdoolaege, G. Karagounis, A. Murari, J. Vega, G. Van Oost
and JET EFDA contributors

Modeling Fusion Data in Probabilistic Metric Spaces: Applications to the Identication of Confinement Regimes and Plasma Disruptions

Modeling Fusion Data in Probabilistic Metric Spaces: Applications to the Identication of Confinement Regimes and Plasma Disruptions

G. Verdoolaege[1], G. Karagounis[1], A. Murari[2], J. Vega[3], G. Van Oost[1]
and JET EFDA contributors*

JET-EFDA, Culham Science Centre, OX14 3DB, Abingdon, UK

[1]Department of Applied Physics, Ghent University, Ghent, Belgium
[2]Associazione EURATOM-ENEA sulla Fusione, Consorzio RFX, Padova, Italy
[3]Laboratorio Nacional de Fusion, Asociacion EURATOM-CIEMAT, Madrid, Spain
** See annex of F. Romanelli et al, "Overview of JET Results", (23rd IAEA Fusion Energy Conference, Daejon, Republic of Korea (2010)).*

Preprint of Paper to be submitted for publication in Proceedings of the
11th Kudowa Summer School, "Towards Fusion Energy"
Kudowa Zdrój, Poland June 11th June - 15th June 2012

ABSTRACT

Pattern recognition is becoming an increasingly important tool for making inferences from the massive amounts of data produced in fusion experiments. In this work, we present an integrated framework for (real-time) pattern recognition for fusion data. The main starting point is the inherent probabilistic nature of measurements of plasma quantities. Since pattern recognition is essentially based on geometric concepts such as the notion of a distance, this necessitates a geometric formalism for probability distributions. To this end, we apply information geometry for calculating geodesic distances on probabilistic manifolds. This provides a natural and theoretically motivated similarity measure between data points for use in pattern recognition techniques. We apply this formalism to classification for the automated identification of plasma confinement regimes in an international database and the prediction of plasma disruptions at JET. We show the distinct advantage in terms of classification performance that is obtained by considering the measurement uncertainty and its geometry. We hence advocate the essential role played by measurement uncertainty for data interpretation in fusion experiments. We finally discuss future applications such as the establishment of scaling laws.

1. INTRODUCTION

Present-day fusion devices generate large amounts of data that are stored in massive databases. A significant potential lies in such data collections for enhancing the physical understanding of fusion plasmas by learning structures or patterns of interest directly from the data and through data visualization for subsequent expert interpretation. Furthermore, real-time data interpretation is indispensable for plasma control and also in this case data-driven approaches can provide considerable benefits. An important feature of the data-driven approach is that no (or few) physical or modelling assumptions are needed in order to derive valuable conclusions from the measurements. It should also be stressed, however, that this does not exclude the incorporation of trustable information regarding the physical model; i.e. the model-based and data-driven approaches can be easily complementary.

In this paper we present a novel integrated framework that tackles various pattern recognition challenges related to fusion data. The aim is to construct an informative representation of complex stochastic data sets that allows an efficient recognition of interesting data patterns and to adapt pattern recognition methods to maximally profit from this representation. Adopting a probabilistic approach, the framework is especially suitable for analysing measurements that are subject to a great deal of uncertainty, such as it can be the case in fusion devices. Hence, we respect the inherent probabilistic nature of the data by developing pattern recognition methods that are able to deal with probability distributions. Pattern recognition essentially relies on geometric concepts such as distance, dispersion and projection. Therefore, our proposed method is based on information geometry, which provides a natural geometric structure to probability spaces. In information geometry a metric tensor on probabilistic manifolds is defined, allowing the calculation of a geodesic distance (GD) between

probability distributions. A key observation in this work is that, in addition to being the proper formalism for treating uncertainty, the probabilistic description of data drastically improves the performance of classification and visualization techniques. We furthermore demonstrate the value of our technique via two applications in a tokamak: the identification of plasma confinement regimes and plasma disruption prediction.

The real-time automated identification of confinement regimes (basically L- and H-mode) has important applications in plasma control and will be an important tool for ITER. In addition, extracted patterns from confinement data, such as clusters of similar plasma regimes, can contribute to the understanding of the physics. Furthermore, the concept of regime identification is closely related to the establishment of scaling laws for the L to H transition power threshold and the energy confinement time. Previous approaches to automated confinement mode identification include the work described in [1], where fuzzy logic and support vector machines were used for the classification of confinement regimes at JET. In [2], support vector machines were applied for classification of confinement modes in the International Tokamak Physics Activity (ITPA) Global H-mode Confinement Database. A neural network classier for JET confinement modes was used in [3]. However, none of the previous methods took a fundamentally probabilistic approach to the subject.

The second application that we study is disruption prediction at JET. Several studies have addressed automated real-time disruption prediction in recent years. The idea is to employ a set of indicator signals representing various physical plasma quantities and to train a learning system to recognize disruptive behaviour on this basis. Provided this can be done sufficiently early before the disruption (typically a few tens of milliseconds), dedicated control systems can take mitigating actions. At JET, encouraging results were obtained with a neural network predictor, but the system was applied to a limited database, while both the success rate and the number of false alarms leave room for improvement [4]. In [5] an extensive database of JET pulses was used for training and testing a support vector machine classier. The system was designed to operate in real time and is based on the observation that disruptive plasma behaviour is characterized by the occurrence of high-frequency components in several representative plasma signals. Although using this system good performances were obtained, there is still considerable interest to improve the performance of automated disruption predictors in general. Particularly critical issues are related to the prediction capability in a more early stage before the time of disruption and in those instances where the plasma conditions differ substantially from those for which the classier was trained (generalization performance). In this work, we employ a set of probabilistic features corresponding to distributions of indicator signals in the wavelet domain and show that this leads to very encouraging results.

The paper is organized as follows. In Section 2 we present the motivation for our probabilistic-geometric framework and the details of the approach. Section 3 discusses the first application to confinement mode discrimination, while Section 4 contains the description and results of the second application to disruption prediction. Section 5 concludes the paper and gives an outlook to future developments.

2. A GEOMETRIC-PROBABILISTIC PATTERN RECOGNITION FRAMEWORK

2.1 PATTERN RECOGNITION FOR FUSION DATA

The term `pattern recognition' encompasses several concepts. Regression refers to learning a|possibly nonlinear| relation between variables. Clustering and classification are used to group data points according to similarity of their characteristics. Searching a database for a pattern in a given query is called information retrieval. All of these tasks basically require a similarity measure or a distance between data points, which is one of the most fundamental concepts in geometry.

Pattern recognition for fusion data is hampered by several data characteristics. First, the databases are vast and pattern learning from large data amounts often requires considerable computational resources. Learning methods therefore need to work sufficiently fast. For instance, a closed-form expression for a similarity measure between data points is very convenient for classification or clustering purposes.

Second, fusion plasmas are described by tens to hundreds of variables. Depending on the organization and representation of the data set, the dimensionality of diagnostic data may run up even more, e.g. when each sample in a signal has its corresponding dimension in the data space. It is well known that learning methods usually perform poorly in data spaces of excessive dimensionality. Therefore, it is essential to reduce the data dimensionality, for instance by projecting the data into a lower-dimensional space, preferably with a minimum of distortion in the configuration of data points.

Third, there is a considerable redundancy between measured quantities due to complex, nonlinear interactions. Data redundancy induces data patterns, which in multidimensional data spaces are manifested through lower-dimensional manifolds, or multidimensional regression surfaces, around which the data points lie scattered. This is the basis of an important class of dimensionality reduction techniques that learn the geometry of such manifolds from the data, which is also strongly linked to regression. However, due to the general nonlinearity of data manifolds, this is a highly challenging enterprise.

Finally, measurements in fusion devices are often subject to a substantial uncertainty, both stochastic (e.g. measurement noise, plasma fluctuations, etc.) and systematic. Classic pattern recognition or statistical methods deal with this uncertainty in a way that somewhat decouples the measurement value from its fundamental uncertainty property. That is, the primary object of interest is usually considered to be the measurement value itself, while its associated error bar or, more comprehensively, its probability distribution, is treated as a side-effect of the measurement process, which ultimately influences the reliability of inferences. In contrast, in our approach the fundamental object is the probability distribution itself, taking full advantage of the extra information that it contains over the measurement value alone. Information on the probability distribution that underlies a measurement can be obtained by fitting a distribution to a set of repeated measurements. Alternatively, error analysis can be applied to derive a measure for the dispersion of the underlying probability distribution. In some cases Gaussian error propagation suffices, but if the forward model is complicated, possibly involving multiple diagnostics, a more advanced error analysis may

be appropriate. A suitable framework to do this is integrated data analysis (IDA) using Bayesian probability theory [6]. Dependencies between physical variables can be captured in a multivariate distribution, although many nonlinear relations are too complex to be efficiently described by tractable probability models. Such relations are better characterized by a dedicated regression analysis.

2.2 THE GEOMETRY OF PROBABILITY DISTRIBUTIONS

For the purpose of the classification and visualization methods presented in this work, a notion of similarity between data points is needed. In a probabilistic description this translates to a similarity measure between probability distributions. This can be obtained within the field of information geometry, where probability density families are interpreted as (Riemannian) differentiable manifolds [7, 8]. A point on the manifold corresponds to a specific probability density function (PDF) within the family and the family parameters provide a coordinate system on the manifold. Cramér [9] and Rao [10] observed that the Fisher information can be regarded as a metric tensor (Fisher-Rao metric) on such a manifold. Once the metric is known, one can establish and solve the geodesic equations, allowing the calculation of the geodesic distances on the manifold [11]. Thus, the geodesic distance (GD) is a natural and theoretically motivated similarity measure between probability distributions. Given a probability model $p(x|\theta)$ for a vector-valued variable x, labelled by an N-dimensional parameter vector θ, the components of the Fisher information matrix $g_{\mu\nu}$ are defined through the relations

$$g_{\mu\nu}(\theta) = -E\left[\frac{\partial^2}{\partial\theta^\mu \partial\theta^\nu} \ln p(x|\theta)\right], \quad \mu,\nu = 1 \ldots N,$$

where the expectation is with respect to the data vector x. In this paper we discuss applications that are based on a univariate Gaussian model (confinement mode identification) and a univariate zero-mean Laplace distribution (disruption prediction).

2.2.1 Univariate Gaussian distribution

The univariate Gaussian distribution, parameterised by its mean μ and standard deviation σ, is defined by the following PDF:

$$p(x|\mu,\sigma) = \frac{1}{\sqrt{2\pi}\sigma} \exp\left[-\frac{(x-\mu)^2}{2\sigma^2}\right].$$

The Fisher-Rao metric can be given via the quadratic line element [12]:

$$ds^2 = \frac{1}{\sigma^2}d\mu^2 + \frac{1}{\sigma^2}d\sigma^2.$$

A closed-form expression exists for the GD, permitting a fast evaluation. Indeed, for two univariate Gaussian distributions $p_1(x|\mu_1, \sigma_1)$ and $p_2(x|\mu_2, \sigma_2)$, parameterised by their mean μ_i and standard deviation σ_i (i = 1, 2), the GD is given by [12]

$$\mathrm{GD}(p_1 \| p_2) = \sqrt{2} \ln \frac{1+\delta}{1-\delta} = 2\sqrt{2} \tanh^{-1} \delta, \qquad \delta \equiv \left[\frac{(\mu_1 - \mu_2)^2 + 2(\sigma_1 - \sigma_2)^2}{(\mu_1 - \mu_2)^2 + 2(\sigma_1 + \sigma_2)^2} \right]^{1/2}.$$

For illustration purposes, an (approximately) isometric embedding of the Gaussian manifold in three-dimensional Euclidean space is shown in Figure 1a. Every point on this surface represents a Gaussian distribution, characterized by a mean and a standard deviation. The Euclidean distance in the three-dimensional Euclidean space between any two points on the surface, equals the true GD between the corresponding distributions. An example of a geodesic between two arbitrary Gaussians is drawn on the surface and the evolution of the distribution along the geodesic is visualized in Figure 1b.

Finally, in the case of multiple independent Gaussian variables it is easy to prove that the square GD between two sets of products of distributions is given by the sum of the squared GDs between corresponding individual distributions [12].

2.2.2 Zero-mean Laplace distribution

The univariate Laplace distribution is a particular case of the generalized Gaussian distribution or GGD (exponential power distribution). The generalized Gaussian distribution is characterized by the PDF

$$p(x|\mu, \sigma, \beta) = \frac{\beta}{\Gamma\left(\frac{1}{2\beta}\right) 2^{\frac{1}{2\beta}} \sigma} \exp\left[-\frac{1}{2} \left(\frac{x-\mu}{\sigma} \right)^{2\beta} \right].$$

Here, $\Gamma(\cdot)$ denotes the Gamma function and $\beta > 0$ is called the shape parameter, which is related to the kurtosis (peakedness) of the distribution. Clearly, $\beta = 1$ yields the univariate Gaussian PDF, while the case of $\beta = 1/2$ is called the Laplace distribution. Note that σ is a dispersion parameter that can be identified with the standard deviation of the distribution only in the Gaussian case. The smaller β, the more peaked the distribution becomes and the heavier its tails, in comparison with the reference Gaussian distribution. The GGD is often used to model wavelet detail statistics, as outlined in Section 4. A plot of a Gaussian and a Laplace distribution fitted to a typical wavelet histogram are shown in Figure 2, with the Laplace distribution clearly providing a better fit.

The information geometry of the family of univariate elliptic distributions, to which the GGD belongs, was studied in [13] and extended to the multivariate case in [14]. Geodesics and geodesic distances for this type of distributions were calculated in [15] and, specifically for the multivariate GGD, in [16, 17] and [11]. Focusing on the univariate zero-mean Laplace distribution with dispersion parameter , the quadratic line element is simply given by

$$\mathrm{d}s^2 = \frac{1}{4} \mathrm{d}\sigma^2.$$

The GD between two zero-mean Laplace distributions $p_1(x|\sigma_1)$ and $p_2(x|\sigma_2)$ then becomes [17]

$$\mathrm{GD}(p_1 \| p_2) = \frac{1}{2} \ln \frac{\sigma_2}{\sigma_1}.$$

3. CONFINEMENT REGIME IDENTIFICATION

Our first application of information geometry to pattern recognition for fusion data is the classification of plasma confinement regimes. At this stage we do not intend to present a dedicated classification platform for application in the field, although the proposed methods can certainly be used for that purpose. Rather, the objective of the experiments discussed here, is to provide a benchmark for classification algorithms that use different data models and similarity measures. This is also important with a view to future work, where we intend to apply our framework to regression for scaling laws.

3.1 ITPA DATABASE

In this work for confinement mode identification we employ measurements from the International Tokamak Physics Activity (ITPA) Global H-mode Confinement Database (DB3, version 13f), henceforth referred to as the `ITPA database' [18, 19]. The ITPA database contains more than 10; 000 validated measurements of various global plasma and engineering variables at one or several time instants during discharges in 19 tokamaks. The data have been used extensively for determining scaling laws for the energy confinement time, mainly as a function of a set of eight plasma and engineering parameters: plasma current, vacuum toroidal magnetic field, total power loss from the plasma (P_{loss}), central line-averaged electron density (n_e), plasma major radius, plasma minor radius, elongation and effective atomic mass. The objective is then to extrapolate to ITER conditions. We used the same eight variables to discriminate between, roughly, L- and H-mode plasmas. Specifically, all database entries with a confinement mode labelled as H, HGELM, HSELM, HGELMH, HSELMH and LHLHL were considered to belong to the H-mode class, while discharges labelled with L, OHM and RI were assigned to the non-H-mode class, or L$\bar{-}$mode for brevity.

The ITPA database lists typical error estimates of measurements for the various plasma and engineering variables. It should be noted that this represents very limited information on the probability distribution underlying each quantity. Furthermore, the interpretation of the error estimates is not always unambiguous and in some cases it is not clear to what extent the estimates are sufficiently reliable for subsequent analysis. Nevertheless, let us assume for the moment that the error bars pertain to a statistical uncertainty in the data, specifically that they represent a single standard deviation. According to the principle of maximum entropy the underlying probability distribution is Gaussian with mean the measurement itself and standard deviation the error bar. Let us also suppose that, for stationary plasma conditions, all variables are statistically independent and so the joint distribution factorizes. Put differently, the joint distribution for the eight variables mentioned above is assumed to be just the product of the individual univariate Gaussian distributions. Clearly, this is a strong assumption and it is imposed here mainly for keeping the calculations tractable. It is also important to note that our formalism has no difficulties with the heterogeneous sources of the measurements, coming from different tokamaks and possibly with different error bars for essentially the same physical quantities. The reason is that the error estimates are automatically embedded in the probabilistic data description.

3.2 DATA VISUALIZATION

A first step towards the identification of patterns in the ITPA database consists of the visualization of the data through a scatter plot in the natural two-dimensional Euclidean space. Since the original data dimensionality is eight, the data visualization involves a dimensionality reduction procedure. This is done using metric multidimensional scaling (MDS), searching for a configuration of points in the Euclidean plane yielding minimal distortion of all pairwise distances. Specifically, suppose the (geodesic) distance in the original data space between data points i and j is d_{ij}, while the coordinate vectors of the corresponding projected points in the reduced Euclidean space are x_i and x_j, respectively. Metric MDS then comes down to an optimization problem, looking for a set of coordinates x_k ($k = 1,..., n$) in the reduced space, for which the following cost function E becomes minimal:

$$E \equiv \sum_{i<j} (\| x_i - x_j \| - d_{ij})^2, \quad i,j = 1, \ldots, n.$$

Here, n is the total number of data points and jj jj refers to the Euclidean norm. Clearly, there is some ambiguity related to the freedom of choice of the reference frame. However, once this is fixed, E has a single global minimum.

Figure 3 shows two approximately isometric projections of the ITPA data into the Euclidean plane, obtained via MDS. For Figure 3a (and 3b) the measurement uncertainty was not considered and MDS was carried out on the basis of simple Euclidean distances in the original data space. On the contrary, the MDS in Figure 3c is based on GDs between Gaussian product distributions. It can be clearly noticed that the projections obtained with the GD, which take into account the measurement error, exhibit considerably more structure compared to the Euclidean case. In particular, it is much easier to visually discriminate between the L- and H-mode clusters. This suggests an important potential of our framework for regression.

3.3 CONFINEMENT MODE CLASSIFICATION

We next performed a series of classification experiments with two classes (L- and H-mode) using 5% of the data for training. We carried out k-nearest neighbour (kNN) classification with $k = 1$, effectively assigning a point to be classified to the class that its nearest neighbour belongs to. The results are shown in Table I. The experiments were performed once without and once with consideration of the measurement error. If all eight plasma parameters are used, the performance of the classifiers is excellent but relatively similar. In order to more clearly show the advantage of the probabilistic approach, we repeated the experiments using only measurements of n_e and P_{loss}. One can see clearly now that the results are better if the measurement error is considered, even using the Euclidean distance. The best results are obtained with the GD, since it properly takes into account the geometry of the probabilistic manifold. It is remarkable that even the approximate and limited information in the ITPA database on the underlying probability distribution is beneficial to the classification

task. The results of a final experiment are also shown, wherein randomized values of the error bars were used (although still within the same range as before). This proves that it is indeed the specific uncertainty information mentioned in the database that contains useful information.

4. DISRUPTION PREDICTION

The methodology behind the application regarding disruption prediction in this work, is based on the experiments described in [5] and we also compare to this method. It has been observed that several plasma signals contain information on the onset of a disruption, both in their absolute value and their frequency content. In this work we only take into account features that are related to the frequency components of the signals obtained via the wavelet transform. Hence, it is important to note that the results should not be compared to the classification performance of other systems in the field. Rather, we intend to demonstrate the superior performance of the wavelet statistical features in conjunction with the GD, compared to Fourier features in a Euclidean space, as in [5].

4.1 WAVELET STATISTICAL FEATURES

Changes in the frequency content of several indicator signals can typically be observed from about 200ms before the time of disruption (ToD) [5]. In addition, in many cases the development of a disruption is accompanied by transient signal features such as spikes, which can be adequately translated into the wavelet domain. Finally, the feature vectors should not depend on specific signal patterns and a statistical framework is best suited.

The one-dimensional discrete wavelet transform of a time-domain signal s(t) is a multi-scale representation defined as follows. Given a `scaling function' $\phi(t)$ (father wavelet) and a `wavelet function' $\psi(t)$ (mother wavelet), both defined in the time domain and of a limited duration, one can construct the scaled and translated variants

$$\varphi_{j,k} = 2^{-j/2}\,\varphi(2^{-j}\,t-k),$$

$$\psi_{j,k} = 2^{-j/2}\,\psi(2^{-j}\,t-k).$$

The signal can then be decomposed in this basis at a prespecified level J as follows:

$$s(t) = \sum_{k} a_{J,k}\,\varphi_{J,k} + \sum_{j\le J}\sum_{k} d_{j,k}\,\psi_{j,k}\,,$$

with the approximation coefficients $a_{j,k}$ and detail coefficients $d_{j,k}$ given by

$$a_{j,k} = \int_{-\infty}^{\infty} s(t)\varphi_{j,k}\,dt,$$

$$d_{j,k} = \int_{-\infty}^{\infty} s(t)\psi_{j,k}\,dt.$$

Intuitively, the detail coefficients measure the local changes of signal levels at a certain scale. We use the statistics of these coefficients to characterize the frequency content of an indicator

signal. Usually most of the detail coefficients are close to zero, since signal changes are relatively rare. Important signal characteristics are therefore located in the heavy tails of the distribution of detail coefficients. This is the reason that often wavelet detail statistics are not well modelled by a Gaussian distribution, whereas a distribution with a higher kurtosis better captures the shape of the distribution. Since an approach using histograms of wavelet coefficients is time-consuming and rather impractical for our purposes, we model wavelet detail coefficients with a Laplace distribution. An example of a wavelet histogram, together with the maximum likelihood t by a Gaussian and a Laplace distribution, is shown in Figure 2.

4.2 DATABASE AND FEATURE EXTRACTION

In previous studies at JET, several physical variables, acquired from a number of dedicated diagnostics, were identified to contain useful information for disruption prediction [5]. The 13 variables used in the present work are listed in Table II. The data were obtained from a series of 582 disruptive JET discharges during campaigns C15–C27 (2004–2009) and the database was compiled in the work described in [5]. The ground truth for the current experiments, i.e. the actual ToD in each disruptive discharge, was determined by a team of experts.

Each plasma signal was resampled to a common time base (1kHz) and normalized to the interval [0; 1]. Since the minimum time required for the actuators at JET to take countermeasures against an upcoming disruption is about 30ms, each time series was then divided in windows of 30 ms duration (30 samples) to mimic the situation of real-time disruption prediction. Non-disruptive features were calculated for each of these intervals up to one second before the ToD (`non-disruptive phase'), while the disruptive features were obtained from the last 210ms before the ToD (`disruptive phase'). The non-decimated (no subsampling) discrete wavelet transform at levels one to three was carried out for each interval and every signal using Daubechies' 4-tap wavelets. Finally a zero-mean Laplacian was t to the wavelet detail coefficients in every subband, and the resulting parameters for all subbands and for all 13 indicator signals in an interval were concatenated into a single feature vector. In calculating the GD between feature vectors, the different plasma signals and wavelet subbands were, again, assumed to be mutually independent. This permitted a pairwise evaluation of the GD between corresponding signals and subbands, with the total squared GD given by the sum of squares of the individual GDs.

In Figure 4 an example for JET Pulse No: 69617 is shown. This discharge disrupted at around 12.78s after a complicated sequence of events, starting with a large sawtooth crash that triggered a neoclassical tearing mode (NTM) which subsequently locked. The rising signal of the mode lock amplitude is shown just before the termination of the discharge, together with the corresponding non-decimated wavelet detail signals at three subsequent scales. The changing statistics of the wavelet detail coefficients can clearly be observed, indicating the appropriateness of the proposed wavelet features for classification.

We compared our results with features based on the Fourier transform of the indicator signals.

Following [5], we calculated the standard deviation of the Fourier power spectra of the signals (excluding the DC component).

4.3 CLASSIFICATION EXPERIMENTS

Again we used a simple k-nearest neighbour classier ($k = 1$), but in a later stage an algorithm that is more tailored to the specific problem can be applied (e.g. more computationally efficient). In a first experiment, data from 334 disruptive pulses from campaigns C15–C20 were employed, with 65% of the data used for training and the rest for testing the classier. The training percentage was chosen to be the ratio above which no significant performance improvement could still be noticed. Note also that the ratio of training samples is much higher than the 5% used for confinement mode classification in Section 3, indicating the different level of difficulty of the classification problems. As mentioned before, we made a comparison with the results of a classier that uses the standard deviations of the Fourier spectra. In the latter case, we first used the Euclidean distance as a similarity measure between the vectors of standard deviations. Second, we treated each as the standard deviation of a zero-mean Gaussian distribution, hence taking into account the probabilistic interpretation of the features.

A good disruption predictor not only should recognize an upcoming disruption, it should also avoid triggering a false alarm, as this would unnecessarily shut down the discharge and waste experimental or operational time. Therefore the performance of every experiment was measured by calculating the true positive rate (TPR, rate of correctly recognized disruptive samples (i.e. windows of 30 ms duration)) and false positive rate (FPR, rate of non-disruptive samples wrongly identified as disruptive) in the testing phase. Furthermore, we measured the rate of pulses for which there was a missed alarm (MA, disruption not detected in disruptive phase), a false alarm (FA, disruption detected in non-disruptive phase). In addition, the success rate (SR = 1– (MA + FA)) was recorded, or the rate of pulses where the disruption was detected in the disruptive phase, as well as the average time (AVG) of the correct detection of a disruption before the ToD.

The results of the classification experiments are shown in Table III. Each experiment, including training and testing, was repeated 20 times and the average rates were calculated. The standard deviation of each of the rates was used as an error estimate and is mentioned in the table as well. It can be clearly observed that for the Fourier features the GD performs better than the Euclidean distance. In addition, our method based on wavelet Laplace features with the GD as a similarity measure, yields still considerably better results.

In a second experiment, we tested the generalization capability of the classifiers. To this end, without performing any further training, we applied the classifiers to data from each of the JET campaigns C21 until C27, from which no data was used for training. The resulting success rates are displayed in Figure 5 for all three classifiers. Again, our method exhibits very promising generalization capabilities for all campaigns.

CONCLUSIONS AND OUTLOOK

We have stressed the important potential of pattern recognition methods for the analysis of fusion data and we have discussed the specific difficulties in the field of nuclear fusion, specifically the strongly stochastic nature of the measurements. We have argued that a fundamentally probabilistic modelling of the data is required. In order to apply pattern recognition to collections of probability distributions, we have employed the formalism of information geometry. This provides a natural distance measure on manifolds of distribution families in the form of the geodesic distance (GD). We have applied a simple k-nearest neighbour classier together with the GD in two entirely different applications: confinement regime identification and disruption prediction. We have obtained classification results where our technique consistently outperforms existing state-of-the-art methods.

It is remarkable that in both our applications there is a clear benefit from the probabilistic description of the data. In the case of the recognition of confinement regimes, the uncertainty information is limited, but apparently still sufficient to aid in the classification task. Hence, not only does our framework allow an intrinsic treatment of the uncertainty information, but also this information itself contributes to the discrimination of confinement modes and disruptive behaviour. This is a strong argument that supports the importance of uncertainty or error estimation for fusion diagnostics. By treating the probability distribution as the fundamental result of the measurement act, not only a single or mean measurement value, we acknowledge this point of view, faithfully taking into account the inherent probabilistic nature of the measurement. Moreover, our framework is not restricted to the traditional Gaussian error estimates, but can deal with any probability model (possibly requiring numerical evaluation of the GD).

Future work will include several aspects of this research. On the one hand, we intend to further expand our geometric-probabilistic pattern recognition framework by addressing other pattern recognition tasks. This includes more sophisticated classification algorithms, as well as dimensionality reduction and regression on probabilistic manifolds. Regression will be very useful for setting up scaling laws where the regression function is intrinsically influenced by all uncertainty information (i.e. the distribution), rather than only depending on a simple weighting of the measurements according to their error bar. On the other hand, we will also adapt the applications to confinement regime identification and disruption prediction so that they can be used in the field as competitive alternatives to the state-of-the-art. Furthermore, we intend to study substructures of the confinement mode classes, which may be linked to specific physical aspects of the confinement, such as edge-localized mode (ELM) types. Likewise, we will investigate whether substructures of a disruptive class of discharges can be linked to different types of disruptions.

ACKNOWLEDGEMENTS

This work was supported by EURATOM and carried out within the framework of the European Fusion Development Agreement. The views and opinions expressed herein do not necessarily re effect those of the European Commission.

REFERENCES

[1]. A. Murari, G. Vagliasindi, M. Zedda, R. Felton, C. Sammon, L. Fortuna, P. Arena, and JET-EFDA Contributors, "Fuzzy logic and support vector machine approaches to regime identification in JET," IEEE Transactions on Plasma Science, vol. **34**, no. 3, pp. 1013–1020, 2006.

[2]. A. Lukianitsa, F. Zhhdanov, and F. Zaitsev, "Analyses of ITER operation mode using the support vector machine technique for plasma discharge classification," Plasma Physics and Controlled Fusion, vol. **50**, no. 6, article no. 065013, 2008.

[3]. A. Meakins, D. M^C Donald, and JET-EFDA Contributors, "The application of classification methods in a data driven investigation of the JET L-H transition," Plasma Physics and Controlled Fusion, vol. **52**, no. 7, article no. 075005, 2010.

[4]. B. Cannas, A. Fanni, P. Sonato, M. Zedda, and JET-EFDA Contributors, "A prediction tool for real-time application in the disruption protection system at JET," Nuclear Fusion, vol. 47, no. 11, pp. 1559{1569, 2007.

[5]. G. Rattá, J. Vega, A. Murari, G. Vagliasindi, M. Johnson, P. De Vries, and JET-EFDA Contributors, "An advanced disruption predictor for JET tested in a simulated real-time environment," Nuclear Fusion, vol. **50**, no. 2, article no. 025005, 2010.

[6]. G. Verdoolaege, R. Fischer, G. Van Oost, and JET-EFDA Contributors, "Potential of a Bayesian integrated determination of the ion effective charge via bremsstrahlung and charge exchange spectroscopy in tokamak plasmas," IEEE Transactions on Plasma Science, vol. **38**, no. 11, pp. 3168{3196, 2010.

[7]. S. Amari and H. Nagaoka, Methods of information geometry, vol. **191** of Transactions of mathematical monographs. New York: American Mathematical Society, 2000.

[8]. R. Kass and P. Vos, Geometrical foundations of asymptotic inference. Wiley Series in Probability and Statistics, New York: Wiley-Interscience, 1997.

[9]. H. Cramér, "A contribution to the theory of statistical estimation," Skandinavisk Aktuarietidskrift, vol. **29**, pp. 85–94, 1946.

[10]. C. Rao, "Information and accuracy attainable in the estimation of statistical parameters," Bull. Calcutta Mathematical Society, vol. **37**, pp. 81–89, 1945.

[11]. G. Verdoolaege and P. Scheunders, "Geodesics on the manifold of multivariate generalized Gaussian distributions with an application to multicomponent texture discrimination," International Journal of Computer Vision, vol. **95**, no. 3, pp. 265–286, 2011.

[12]. J. Burbea and C. Rao, "Entropy differential metric, distance and divergence measures in probability spaces: a unified approach," Journal of Multivariate Analysis, vol. **12**, no. 4, pp. 575–596, 1982.

[13]. A. Mitchell, "Statistical manifolds of univariate elliptic distributions," International Statistical Review, vol. **56**, no. 1, pp. 1–16, 1988.

[14]. A. Mitchell, "The information matrix, skewness tensor and -connections for the general multivariate elliptic distribution," Annex International Statistical Review., vol. **41**, no. 2, pp. 289–304, 1989.

[15]. M. Berkane, K. Oden, and P. Bentler, "Geodesic estimation in elliptical distributions," Journal of Multivariate Analysis, vol. 63, no. 1, pp. 35–46, 1997.

[16]. G. Verdoolaege, S. De Backer, and P. Scheunders, "Multiscale colour texture retrieval using the geodesic distance between multivariate generalized Gaussian models," in Proceedings of the IEEE International Conference on Image Processing, (San Diego, CA), pp. 169–172, 2008.

[17]. G. Verdoolaege and P. Scheunders, "On the geometry of multivariate generalized Gaussian models," Journal of Mathematical Imaging and Vision, vol. **43**, no. 3, pp. 180–193, 2011.

[18]. D. M^{C}Donald et al., "Recent progress on the development and analysis of the ITPA global H-mode confinement database," Nuclear Fusion, vol. **47**, no. 3, pp. 147–174, 2007.

[19]. http://efdasql.ipp.mpg.de/hmodepublic.

Variables	Mode	Euclidean w/o errors	Euclidean with errors	GD with errors	GD with random errors
All 8	L	96.2	97.4	98.3	94.5
	H	94.1	95.4	97.7	92.3
$\bar{n}_e$, P_{loss}	L	85.1	87.7	91.0	82.4
	H	88.6	89.4	93.0	86.0

Table I: Correct classication rates (%) of connement regimes using a kNN classier for dierent sets of variables, Euclidean and geodesic distance measures and with or without consideration of the uncertainty information.

	Signal name	Unit
(1)	Plasma current	A
(2)	Poloidal beta	
(3)	Time derivative of (2)	s^{-1}
(4)	Mode lock amplitude	T
(5)	Safety factor at 95% of minor radius	
(6)	Time derivative of (5)	s^{-1}
(7)	Total input power	W
(8)	Plasma internal inductance	
(9)	Time derivative of (8)	s^{-1}
(10)	Plasma vertical centroid position	m
(11)	Plasma density	m^{-3}
(12)	Stored diamagnetic energy time derivative	W
(13)	Net power (input minus radiated power)	W

Table II: List of physical variables used for feature extraction.

Performance measure	Fourier Euclidean	Fourier GD	Wavelet GD
TPR (%)	73.5 ± 2.7	81.6 ± 2.2	94.2 ± 1.6
FPR (%)	23.2 ± 3.2	24.0 ± 2.9	5.9 ± 2.2
MA (%)	1.0 ± 0.9	0.6 ± 0.8	0.7 ± 0.7
FA (%)	62.2 ± 6.9	61.3 ± 4.9	10.7 ± 3.1
SR (%)	36.8 ± 6.8	38.1 ± 4.7	88.5 ± 3.2
AVG (ms)	166.3 ± 9.2	174.3 ± 6.6	184.9 ± 2.9

Table III: Results for kNN classication experiments with non-disruptive and disruptive features for JET campaigns C15{C20. Fourier and wavelet statistical features were used, with the Euclidean distance and GD as similarity measures. The experiments were each repeated 20 times, resulting in sample standard deviations that are mentioned as well.

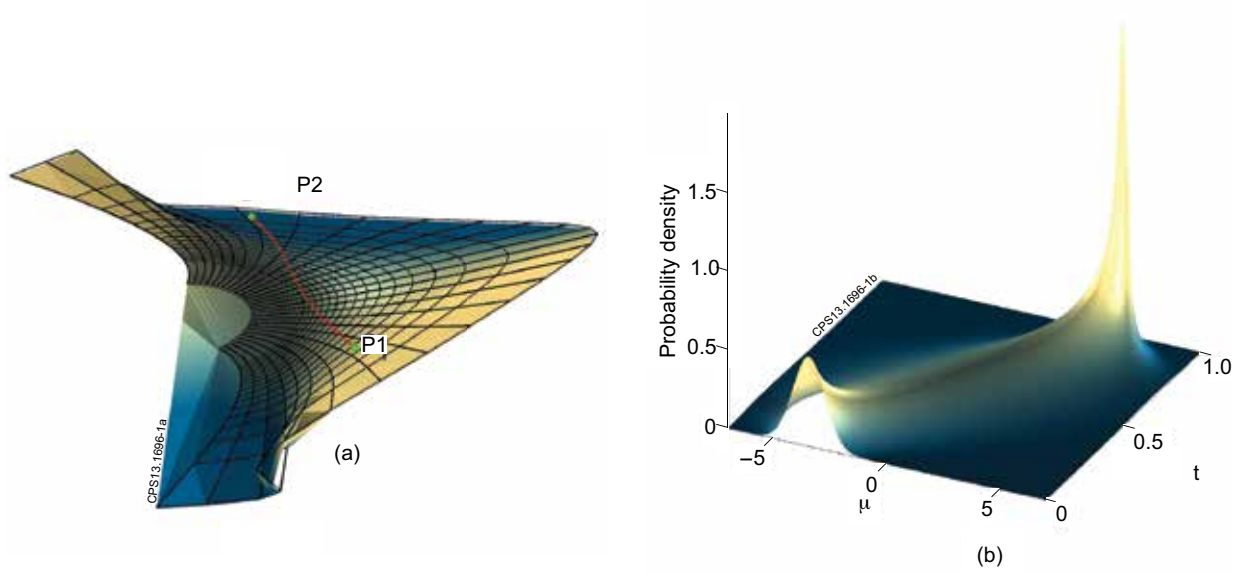

Figure 1: (a) Embedding of the univariate Gaussian manifold and geodesic between two arbitrary Gaussians $p_1(\mu_1 = -4, \sigma_1 = 0.7)$ and $p_2(\mu_2 = 3, \sigma_2 = 0{:}2)$. The full lines are curves of constant mean, the dashed lines are curves of constant standard deviation. (b) Visualization of the distributions along the geodesic, parameterized by t. Each slice along the t-axis shows the distribution at the corresponding point on the geodesic.

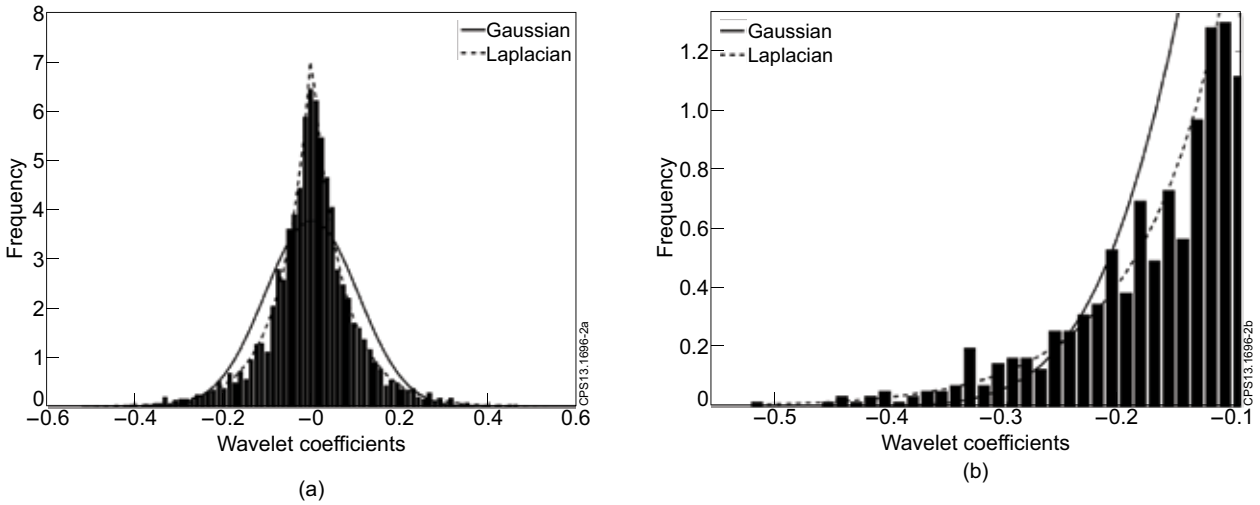

Figure 2: (a) Typical heavy-tailed wavelet detail histogram, together with the best-t Gaussian and Laplace distribution obtained via maximum likelihood. (b) Zoomed display of (a), clearly showing the better t of the tails by the Laplace distribution compared to the Gaussian t.

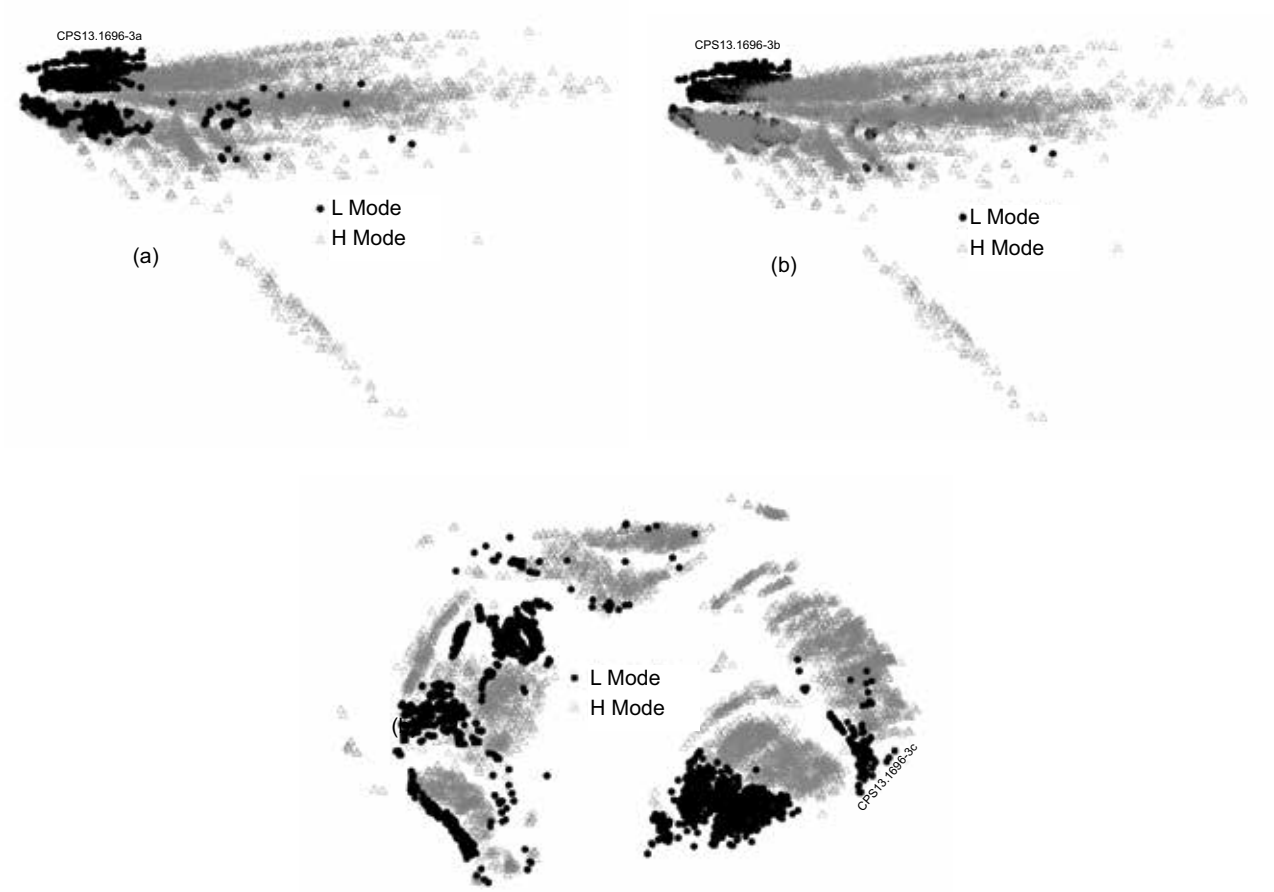

Figure 3: Two-dimensional projections of the ITPA data using MDS, with indicated L- and H-mode clusters. (a) Using the Euclidean distance without measurement error and with the L-mode points on top. (b) The same, but with the H-mode points on top for better visibility. (c) Using the GD with measurement error.

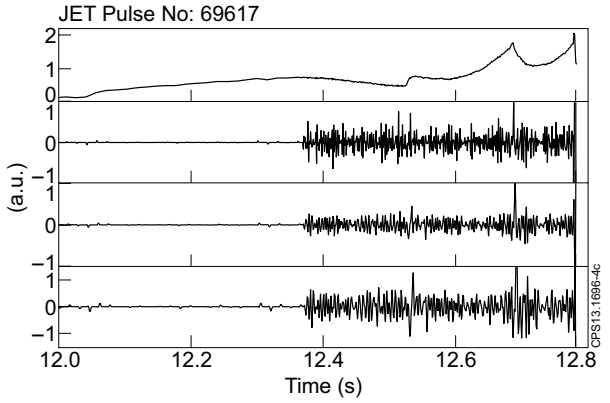

Figure 4: From top to bottom, the panels show the mode lock amplitude and the corresponding non-decimated wavelet detail signals at scales 1, 2 and 3, respectively, for JET Pulse No: 69617.

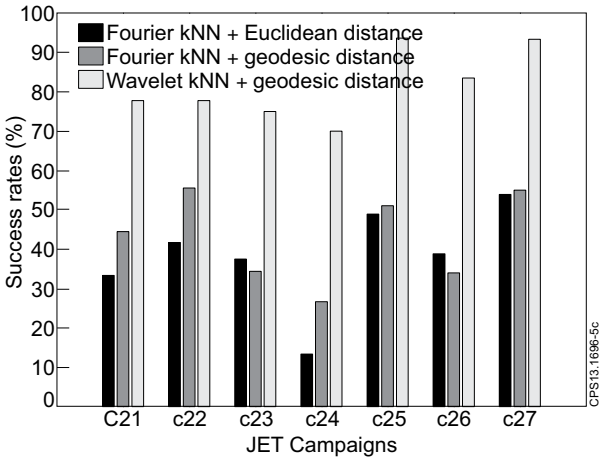

Figure 5: Success rates of the classiers for generalization to each of the campaigns C21 until C27.